Lineshape of the compact fully heavy tetraquark

Zejian Zhuang,[1,2,§] Ying Zhang,[1,2,†] Yuanzhuo Ma®,[1,2,‡] and Qian Wang®[1,2,3,*]

[1]*Guangdong Provincial Key Laboratory of Nuclear Science, Institute of Quantum Matter,*
South China Normal University, Guangzhou 510006, China
[2]*Guangdong-Hong Kong Joint Laboratory of Quantum Matter,*
Southern Nuclear Science Computing Center, South China Normal University,
Guangzhou 510006, China
[3]*Institute of High Energy Physics, Chinese Academy of Sciences, Beijing 100049, China*

Hadrons and their distributions are the most direct observables in experiments, which would shed light on the nonperturbative mystery of quantum chromodynamics. As the result, any new hadron will challenge our current knowledge on the one hand, and provide additional inputs on the other hand. The fully heavy $cc\bar{c}\bar{c}$ system observed by LHCb recently opened a new era for hadron physics. We first extract the internal structure of the fully heavy tetraquarks directly from the experimental data, within the compact tetraquark picture. By fitting to the di-J/ψ lineshape, we find that the $X(6900)$ is only the cusp effect from the $J/\psi\psi(3770)$ channel. In addition, there is also a cusp slightly below 6.8 GeV stemming from the $J/\psi\psi'$ channel. The two 0^{++} tetraquarks behave as two resonances above the di-η_c and di-J/ψ threshold, respectively. The 2^{++} state is a bound state below the di-J/ψ threshold. Furthermore, we find that the $X_{0^{++}}(6035)$ shows a significant structure in the di-η_c lineshape even after the coupled channel effect. This is an unique feature which can distinguish compact $cc\bar{c}\bar{c}$ tetraquark from the loosely hadronic molecules.

DOI: 10.1103/PhysRevD.105.054026

I. INTRODUCTION

The formation of hadrons is from the nonperturbative mechanism of quantum chromodynamics (QCD), the theory of strong interaction. As the result, the properties of hadrons are expected to shed light on the mystery of nonperturbative dynamics of QCD. The success of the conventional quark model prompted the community to search for the predicted missing particles for several decades. The situation breaks up since the observation of the $X(3872)$, as the first exotic candidate, in 2003. That challenges the conventional quark model and stimulates research enthusiasm on the so-called exotic hadrons. Up to now, tens of exotic candidates have been observed by experimental collaborations (such as LHCb, BESIII, BelleII, JLab, CMS, and ATLAS) and numerous studies [1–10] have been proposed for the understanding of their properties.

*[*]Corresponding author.
qianwang@m.scnu.edu.cn
[†]zhangying@m.scnu.edu.cn
[‡]yuanzhuoma@m.scnu.edu.cn
[§]zejian.zhuang@m.scnu.edu.cn

Most of them contain a pair of heavy quarks and are located at the heavy quarkonium region. Two competitive scenarios, i.e., tetraquark and hadronic molecular pictures, are proposed for their nature based on two clusters, i.e., $cq - \bar{c}\bar{q}'$ and $c\bar{q} - \bar{c}q'$, respectively. Although great efforts have been put forward to distinguish these two interpretations for a given particle, there is no definite conclusion about any particle yet in the community. One potential solution is pinning the hope on a fully heavy system, which is one goal of several experimental collaborations, e.g., the LHCb [11,12] and CMS [13] Collaborations. The importance of the fully heavy system is because it cannot be classified to several clusters intuitively. One expects that a comparison of the fully heavy system with the $c\bar{c}q\bar{q}'$ system would give some hints for the formation of hadrons. Luckily, the LHCb Collaboration [12], recently, reported a narrow structure around 6.9 GeV and a broad structure within the range 6.2–6.8 GeV in the di-J/ψ invariant mass distribution, using the data at 7, 8 and 13 TeV center-of-mass energies. Because of the observed channel, the quark content of those structures is $cc\bar{c}\bar{c}$. The narrow structure around 6.9 GeV can be explained by a Breit-Wigner parametrization with and without the interference between the resonant contribution and the nonresonant contribution [12]. This structure is named as the $X(6900)$.

The study of the fully heavy system goes back to 1970s and was motivated by the observation of the ψ' [14] and the

severe emerging structures in e^+e^- annihilation [15]. However, the study becomes a dilemma because of no experimental data. The observation of the $X(6900)$ [12] breaks through the situation. Because of the equal masses of the components, the hadron with $cc\bar{c}\bar{c}$ quarks is more expected to be a compact one [16–47]. However, none of them fit the di-J/ψ lineshape within this scenario, analogous to that within the molecular picture [48–55]. As we know, the experimental events distribution is the most direct input for theoretical analysis and can provide the underlying structure of the interested hadrons, even for the compact object [5,56].

In this work, we first fit the di-J/ψ lineshape with the compact tetraquark picture and extract the corresponding pole positions. The bare pole positions are extracted from a parametrization with both chromoelectric and chromomagnetic interactions. This study can tell to which extent the compact tetraquark picture can explain the lineshape directly.

II. FRAMEWORK

A. Hamiltonian

The interaction in the fully heavy tetraquark system can be described by both chromoelectric and chromomagnetic interaction among the constituent quarks, i.e.,

$$H = \sum_i (m_i + T_i) + \sum_{i<j}\left[A_{ij}\lambda_i \cdot \lambda_j + \frac{B_{ij}}{m_i m_j}\lambda_i \cdot \lambda_j S_i \cdot S_j\right]$$
(1)

where m_i, $S_i = \frac{1}{2}\sigma_i$, λ_i, and T_i are mass, spin matrix, Gell-Mann matrix, and kinematic energy for the ith quark, respectively. For the antiquark, λ_i is replaced by $-\lambda_i^*$. The expected values of A_{ij} and B_{ij} will be extracted from hadrons. Because of the nonrelativistic property of the fully heavy system, we take the nonrelativistic approximation here, i.e., neglecting the kinematic terms in Eq. (1).

B. Wave functions of heavy tetraquark system

Before proceeding to the solutions of the Hamiltonian of Eq. (1), one needs to analyze the wave function of the fully heavy tetraquark system. The total wave function of a tetraquark system is constructed by space, flavor, spin, and color wave functions individually, i.e., the total wave function

$$|\psi\rangle = |\text{space}\rangle \otimes |\text{flavor}\rangle \otimes |\text{spin}\rangle \otimes |\text{color}\rangle. \quad (2)$$

In this work, as we only focus on the ground S-wave fully heavy tetraquarks, the spatial wave function is symmetric and negligible. Thus, we first construct the spin-color wave function in the diquark-antidiquark configuration. Here, $|(Q_1 Q_2)_{S_{12}}, (\bar{Q}_3\bar{Q}_4)_{S_{34}}\rangle_S$ are the spin wave functions with

subscripts S_{12}, S_{34} and S the total spins of the first two quarks, the latter two antiquarks and the sum of them, respectively. The spin wave functions for various J^{PC}'s are listed below

(1) $J^{PC} = 0^{++}$:

$$|(Q_1Q_2)_0, (\bar{Q}_3\bar{Q}_4)_0\rangle_0, |(Q_1Q_2)_1, (\bar{Q}_3\bar{Q}_4)_1\rangle_0, \quad (3)$$

(2) $J^{PC} = 1^{+-}$:

$$|(Q_1Q_2)_1, (\bar{Q}_3\bar{Q}_4)_1\rangle_1$$
$$\frac{1}{\sqrt{2}}[|(Q_1Q_2)_1, (\bar{Q}_3\bar{Q}_4)_0\rangle_1 - |(Q_1Q_2)_0, (\bar{Q}_3\bar{Q}_4)_1\rangle_1],$$
(4)

(3) $J^{PC} = 1^{++}$:

$$\frac{1}{\sqrt{2}}(|(Q_1Q_2)_1, (\bar{Q}_3\bar{Q}_4)_0\rangle_1 + |(Q_1Q_2)_0, (\bar{Q}_3\bar{Q}_4)_1\rangle_1),$$
(5)

(4) $J^{PC} = 2^{++}$:

$$|(Q_1Q_2)_1, (\bar{Q}_3\bar{Q}_4)_1\rangle_2. \quad (6)$$

As we only consider S-wave fully tetraquark system in this work, the orbital angular momentum does not appear in the above equations. The color confinement tells us that all the observed hadrons are a color singlet, which gives the potential color wave functions below

$$|(Q_1Q_2)^6, (\bar{Q}_3\bar{Q}_4)^{\bar{6}}\rangle^1, \quad (7)$$

$$|(Q_1Q_2)^{\bar{3}}, (\bar{Q}_3\bar{Q}_4)^3\rangle^1. \quad (8)$$

Here the superscripts $6(\bar{6})$ and $\bar{3}(3)$ denote the corresponding irreducible representations of the color SU(3) group for diquark (antidiquark). Accordingly, 1 stands for the color singlet. In total, the spatial and color wave functions of the S-wave ground fully heavy systems are symmetric and antisymmetric, which leaves the product of spin and flavor wave functions symmetric due to the Pauli principle. The flavor wave function is symmetric for full-charm (bottom) tetraquarks and could be symmetric or antisymmetric for the $bc\bar{b}\bar{c}$ tetraquarks. As a result, all the potential total wave functions for various J^{PC} are collected in Table I.

C. Parameters

In this work, we do not aim at solving the Schrödinger equation explicitly, but we use a parametrization scheme to extract the mass spectra of the S-wave ground fully heavy tetraquarks. Thus, to investigate the mass spectra, the expectation values of the parameters A_{ij} and B_{ij} for various

TABLE I. The bases of fully heavy tetraquarks, where {} and [] denote the symmetric and antisymmetric flavor functions, respectively, of diquark (antidiquark). The subscripts and superscripts are for the irreducible representations in spin and color spaces, respectively.

J^{PC}	Tetraquark	Wave Function	
0^{++}	$cc\bar{c}\bar{c}$	$\lvert\{cc\}_0^6\{\bar{c}\bar{c}\}_0^{\bar{6}}\rangle_0^1$	$\lvert\{cc\}_1^3\{\bar{c}\bar{c}\}_1^{\bar{3}}\rangle_0^1$
	$bb\bar{b}\bar{b}$	$\lvert\{bb\}_0^6\{\bar{b}\bar{b}\}_0^{\bar{6}}\rangle_0^1$	$\lvert\{bb\}_1^3\{\bar{b}\bar{b}\}_1^{\bar{3}}\rangle_0^1$
	$bc\bar{b}\bar{c}$	$\lvert[bc]_1^6[\bar{b}\bar{c}]_1^{\bar{6}}\rangle_0^1$	$\lvert\{bc\}_0^6\{\bar{b}\bar{c}\}_0^{\bar{6}}\rangle_0^1$
		$\lvert\{bc\}_1^3\{\bar{b}\bar{c}\}_1^{\bar{3}}\rangle_0^1$	$\lvert[bc]_0^3[\bar{b}\bar{c}]_0^{\bar{3}}\rangle_0^1$
1^{+-}	$cc\bar{c}\bar{c}$	$\lvert\{cc\}_1^3\{\bar{c}\bar{c}\}_1^{\bar{3}}\rangle_1^1$	
	$bb\bar{b}\bar{b}$	$\lvert\{bb\}_1^3\{\bar{b}\bar{b}\}_1^{\bar{3}}\rangle_1^1$	
	$bc\bar{b}\bar{c}$	$\lvert[bc]_1^6[\bar{b}\bar{c}]_1^{\bar{6}}\rangle_1^1$	$\frac{1}{\sqrt{2}}\left(\lvert[bc]_1^6\{\bar{b}\bar{c}\}_0^{\bar{6}}\rangle_1^1 - \lvert\{bc\}_0^6[\bar{b}\bar{c}]_1^{\bar{6}}\rangle_1^1\right)$
		$\lvert\{bc\}_1^3\{\bar{b}\bar{c}\}_1^{\bar{3}}\rangle_1^1$	$\frac{1}{\sqrt{2}}\left(\lvert\{bc\}_1^3[\bar{b}\bar{c}]_0^{\bar{3}}\rangle_1^1 - \lvert[bc]_0^3\{\bar{b}\bar{c}\}_1^{\bar{3}}\rangle_1^1\right)$
1^{++}	$bc\bar{b}\bar{c}$	$\frac{1}{\sqrt{2}}\left(\lvert[bc]_1^6\{\bar{b}\bar{c}\}_0^{\bar{6}}\rangle_1^1 + \lvert\{bc\}_0^6[\bar{b}\bar{c}]_1^{\bar{6}}\rangle_1^1\right)$	$\frac{1}{\sqrt{2}}\left(\lvert\{bc\}_1^3[\bar{b}\bar{c}]_0^{\bar{3}}\rangle_1^1 + \lvert[bc]_0^3\{\bar{b}\bar{c}\}_1^{\bar{3}}\rangle_1^1\right)$
2^{++}	$cc\bar{c}\bar{c}$	$\lvert\{cc\}_1^3\{\bar{c}\bar{c}\}_1^{\bar{3}}\rangle_2^1$	
	$bb\bar{b}\bar{b}$	$\lvert\{bb\}_1^3\{\bar{b}\bar{b}\}_1^{\bar{3}}\rangle_2^1$	
	$bc\bar{b}\bar{c}$	$\lvert[bc]_1^6[\bar{b}\bar{c}]_1^{\bar{6}}\rangle_2^1$	$\lvert\{bc\}_1^3\{\bar{b}\bar{c}\}_1^{\bar{3}}\rangle_2^1$

systems should be extracted. As discussed above, the contributions from color and spin spaces have been factorized out by the λ and S matrixes, respectively. In addition, the contribution of the flavor part can be obtained via the corresponding flavor wave functions in Table I. The residue contribution is only from the spacial part via

$$\mathcal{A}_{ij} := \langle A_{ij}\rangle \qquad (9)$$

$$\mathcal{B}_{ij} := \langle B_{ij}\rangle, \qquad (10)$$

with $\langle\cdots\rangle$ the expected values of the spacial wave functions. As we only consider S-wave ground tetraquarks, the expected values can be approximated constants and extracted from S-wave ground pseudoscalar and vector mesons. Because of the symmetry of color and spin spaces, these expected values have the relation

$$\mathcal{A}_{12} = \mathcal{A}_{34}, \qquad \mathcal{A}_{13} = \mathcal{A}_{24} = \mathcal{A}_{14} = \mathcal{A}_{23}, \quad (11)$$

$$\mathcal{B}_{12} = \mathcal{B}_{34}, \qquad \mathcal{B}_{13} = \mathcal{B}_{24} = \mathcal{B}_{14} = \mathcal{B}_{23}. \quad (12)$$

For the parameters $\mathcal{A}_{bc}$ and $\mathcal{B}_{bc}$, the masses of either $c\bar{b}$ or $b\bar{c}$ mesons are indicated as inputs. However, only one $c\bar{b}$ state, i.e., B_c, is observed in experiments [57,58]. Alternatively, the theoretical results of Ref. [59] are used as an input. All the input masses are collected in Table II. Here the heavy quark masses m_i are fixed to the values

$$m_c = 1.5 \text{ GeV}, \qquad m_b = 5 \text{ GeV}, \qquad (13)$$

in the constituent quark model [60]. In the end, the mass formulas for extracting parameters are

$$M_0 = \sum_{i=c,b} m_i + \sum_{i,j=c,b}\left[\frac{-16}{3}\mathcal{A}_{ij} + \frac{4\mathcal{B}_{ij}}{m_i m_j}\right], \quad (14)$$

$$M_1 = \sum_{i=c,b} m_i + \sum_{i,j=c,b}\left[\frac{-16}{3}\mathcal{A}_{ij} + \frac{-4}{3}\frac{\mathcal{B}_{ij}}{m_i m_j}\right], \quad (15)$$

where M_0 and M_1 are the masses of the pseudoscalar and vector meson, respectively. With Eqs. (14) and (15), the parameters $\mathcal{A}_{ij}$ and $\mathcal{B}_{ij}$ can be obtained and listed in Table III. Before proceeding, we also check the applicability of our framework by applying it to triply heavy baryon systems. In the same framework, we obtain the mass formulas

$$M_{\frac{1}{2}} = 2m_Q + m_{Q'} - \frac{8}{3}(2\mathcal{A}_{QQ'} + \mathcal{A}_{QQ}) + \left(-\frac{8}{3}\right)\left(\frac{\mathcal{B}_{QQ}}{4m_Q^2} - \frac{\mathcal{B}_{QQ'}}{m_Q m_{Q'}}\right) \qquad (16)$$

$$M_{\frac{3}{2}} = 2m_Q + m_{Q'} - \frac{8}{3}(2\mathcal{A}_{QQ'} + \mathcal{A}_{QQ}) + \left(-\frac{8}{3}\right)\frac{1}{4}\left(\frac{\mathcal{B}_{QQ}}{m_Q^2} + \frac{2\mathcal{B}_{QQ'}}{m_Q m_Q'}\right) \qquad (17)$$

for $J = \frac{1}{2}, \frac{3}{2}$ QQQ' heavy baryons and

$$M_{\frac{3}{2}} = 3m_Q - \frac{8}{3}\left(3\mathcal{A}_{QQ} + \frac{3}{4}\frac{\mathcal{B}_{QQ}}{m_{QQ}^2}\right) \qquad (18)$$

for $J = \frac{3}{2}$ QQQ heavy baryons. With the extracted parameters, we obtain the masses of the $\Omega_{ccb}^{(*)}$, $\Omega_{bbc}^{(*)}$, Ω_{ccc}^*, and

TABLE II. Masses and errors of heavy mesons used for extracting the parameters. The values of the first four mesons are extracted from Ref. [64].

Mass (MeV)	η_c	J/ψ	η_b	Υ	B_c [59]	B_c^* [59]
m	2983.9	3096.9	9398.7	9460.3	6276	6331
Δm	0.4	0.006	2	0.26	7	7

TABLE III. The values and errors of the parameters $\mathcal{A}_{ij}$ and $\mathcal{B}_{ij}$ in this work.

Parameters	$\mathcal{A}_{QQ^{(\prime)}}$ [GeV]			$\mathcal{B}_{QQ^{(\prime)}}$ [GeV]^3		
	$\mathcal{A}_{cc}$	$\mathcal{A}_{bb}$	$\mathcal{A}_{cb}$	$\mathcal{B}_{cc}$	$\mathcal{B}_{bb}$	$\mathcal{B}_{cb}$
Value	-0.01287	0.10408	0.03427	-0.04767	-0.28875	-0.07734
Error	2×10^{-5}	10^{-4}	1.04×10^{-3}	2.1×10^{-4}	9.45×10^{-3}	1.392×10^{-2}

Ω_{bbb}^* and compare them with the predicted results by lattice QCD simulation [61–63] as shown in Fig. 1. From Fig. 1, one can see that the masses of triply heavy baryons are very close to results given by lattice QCD, which indicates the applicability of our framework.

III. NUMERICAL RESULTS AND DISCUSSIONS

A. Mass spectra of fully heavy tetraquark system with the nonrelativistic parametrization

With all the parameters extracted from the S-wave ground pseudoscalar and vector heavy mesons, one can obtain the matrix elements of the Hamiltonian, i.e., Eq. (1) in the bases listed in Table I. After diagonalizing the Hamiltonian, one can obtain the mass spectra and eigenvectors which can be found in Table IV. To get an intuitive impression of the bare tetraquarks, we also plot the mass
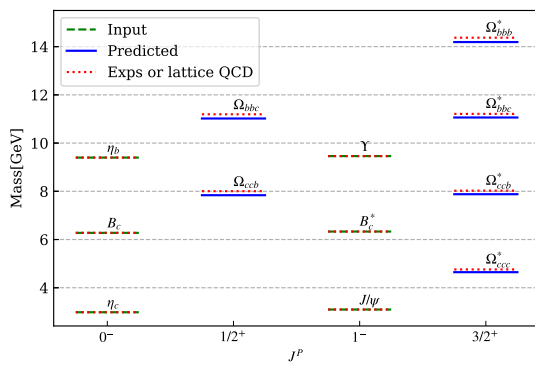

FIG. 1. The comparison of normal heavy hadrons with the predicted values from our framework. The red dotted lines are results from either the PDG or lattice QCD group. The green dashed and blue solid lines are our inputs and predictions, respectively. The values of J/ψ, η_c, Υ, and η_b masses are from PDG [64]. Those of $B_c^{(*)}$, $\Omega_{bbc}^{(*)}$ and $\Omega_{ccb}^{(*)}$ are from Ref. [63]. The masses of Ω_{bbb}^* and Ω_{ccc}^* are from Ref. [61] and Ref. [62], respectively.

spectra of $cc\bar{c}\bar{c}$, $bb\bar{b}\bar{b}$, $bc\bar{b}\bar{c}$, and their potential hidden charm decay channels in Fig. 2. One can see that most of them are above the lowest allowed decay channels and are expected to illustrate themselves as broader structures. However, this expectation might be invalidated due to the couplings of the decay channels as discussed below.

B. Partial decay width of bare fully heavy tetraquarks

As discussed in the above section, most of the bare fully heavy tetraquarks are above their lowest allowed hidden charm/bottom decay channels [16–29,65–69]. As a result, we will discuss their partial widths of hidden charm/bottom channels. As our framework considers all the possible two-body interactions among the four constituents, the $Q_1 Q_2 \otimes \bar{Q}_3 \bar{Q}_4$ base is equal to the $Q_1 \bar{Q}_3 \otimes Q_2 \bar{Q}_4$ (or $Q_1 \bar{Q}_4 \otimes Q_2 \bar{Q}_3$) base. These two bases can be transformed to each other by the Fierz rearrangement [70–72]

$$|\{cc\}_0^6\{\bar{c}\bar{c}\}_0^{\bar{6}}\rangle_0^1 = \frac{1}{2\sqrt{3}}|\{c\bar{c}\}_0^8\{c\bar{c}\}_0^8\rangle_0^1 + \frac{1}{2}|[c\bar{c}]_1^8[c\bar{c}]_1^8\rangle_0^1$$
$$+ \sqrt{\frac{1}{6}}|[c\bar{c}]_0^1[c\bar{c}]_0^1\rangle_0^1 + \sqrt{\frac{1}{2}}|\{c\bar{c}\}_1^1\{c\bar{c}\}_1^1\rangle_0^1,$$

$$|\{cc\}_1^{\bar{3}}\{\bar{c}\bar{c}\}_1^3\rangle_0^1 = -\sqrt{\frac{1}{2}}|\{c\bar{c}\}_0^8\{c\bar{c}\}_0^8\rangle_0^1 + \sqrt{\frac{1}{6}}|[c\bar{c}]_1^8[c\bar{c}]_1^8\rangle_0^1$$
$$+ \frac{1}{2}|[c\bar{c}]_0^1[c\bar{c}]_0^1\rangle_0^1 - \frac{1}{2\sqrt{3}}|\{c\bar{c}\}_1^1\{c\bar{c}\}_1^1\rangle_0^1,$$

$$|\{cc\}_1^{\bar{3}}\{\bar{c}\bar{c}\}_1^3\rangle_1^1 = -\sqrt{\frac{1}{3}}|\{c\bar{c}\}_0^8[c\bar{c}]_1^8\rangle_1^1 - \sqrt{\frac{1}{3}}|[c\bar{c}]_1^8\{c\bar{c}\}_0^8\rangle_1^1$$
$$+ \sqrt{\frac{1}{6}}|[c\bar{c}]_1^1\{c\bar{c}\}_0^1\rangle_1^1 + \sqrt{\frac{1}{6}}|\{c\bar{c}\}_0^1[c\bar{c}]_1^1\rangle_1^1,$$

$$|\{cc\}_1^{\bar{3}}\{\bar{c}\bar{c}\}_1^3\rangle_2^1 = \sqrt{\frac{1}{3}}|\{c\bar{c}\}_1^1\{c\bar{c}\}_1^1\rangle_2^1 - \sqrt{\frac{2}{3}}|[c\bar{c}]_1^8[c\bar{c}]_1^8\rangle_2^1.$$
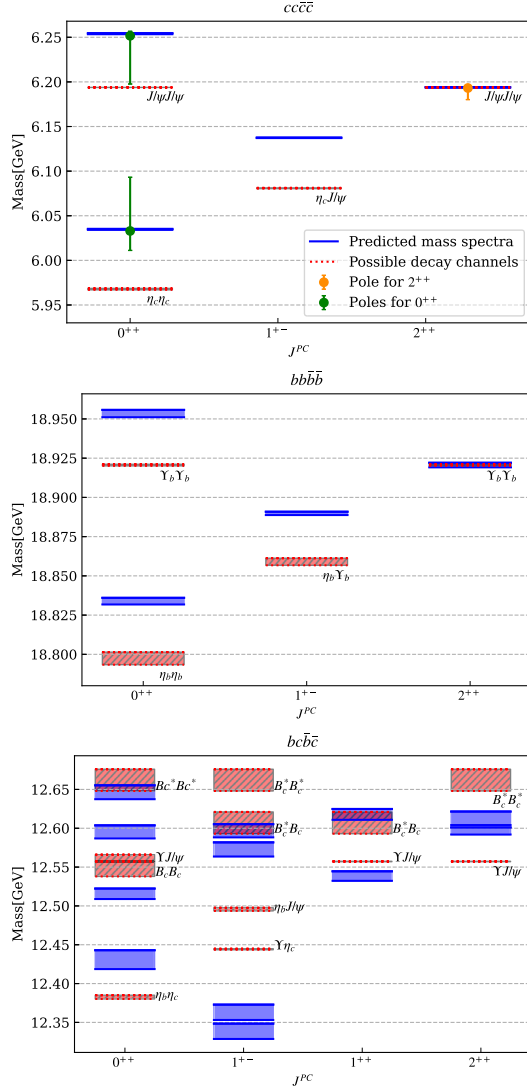
FIG. 2. Mass spectra (blue solid boxes) of $cc\bar{c}\bar{c}$, $bb\bar{b}\bar{b}$, and $bc\bar{b}\bar{c}$ tetraquarks for different J^{PC}'s and their potential hidden charm decay channels (red dashed boxes). The bands are uncertainties either from the framework or the experimental data. The green and yellow points are the poles after the coupled channel effect, which will be discussed in the next sections. The errors inherit from the experimental data.

Here we use the $cc\bar{c}\bar{c}$ system as an example and the transformation for other systems are analogous. Because the observed hadrons are a color singlet, only the $|(c\bar{c})^1(c\bar{c})^1\rangle^1$ components on the right-hand side of the above equations contribute to the hidden charm decay channels. Here $(c\bar{c})$ means either $\{c\bar{c}\}$ or $[c\bar{c}]$ and this depends on the spin of the $c\bar{c}$ pair. The coefficient of the $|(c\bar{c})^1_{s_{i1}}(c\bar{c})^1_{s_{i2}}\rangle^1_{J^{PC}_n}$ component is denoted as α^i_n. Here i indicates the allowed two-body charmonium decay channels. s_{i1} and s_{i2} are the spins of the two $c\bar{c}$ pairs in the ith channel. The subscript J^{PC}_n means the nth J^{PC} base.

The two physical 0^{++} tetraquarks are a combination of the first two bases with the mixing coefficients listed in the last column of Table IV. Collect these coefficients into a matrix as

$$\beta = \begin{pmatrix} 0.58 & 0.81 \\ -0.81 & 0.58 \end{pmatrix}. \tag{19}$$

With all the pieces ready, the transition rates of physical tetraquarks to two hidden charmonium channels can be read through the coefficient matrixes

$$\mu(X_{0^{++}}(6035)) = \left(\sqrt{\tfrac{1}{6}}\beta_{11} + \tfrac{1}{2}\beta_{12} \quad \sqrt{\tfrac{1}{2}}\beta_{11} - \tfrac{1}{2\sqrt{3}}\beta_{12} \right)$$

$$\mu(X_{0^{++}}(6254)) = \left(\sqrt{\tfrac{1}{6}}\beta_{21} + \tfrac{1}{2}\beta_{22} \quad \sqrt{\tfrac{1}{2}}\beta_{21} - \tfrac{1}{2\sqrt{3}}\beta_{22} \right)$$

in the $|[c\bar{c}]^1_0[c\bar{c}]^1_0\rangle^1_0$, $|\{c\bar{c}\}^1_1\{c\bar{c}\}^1_1\rangle^1_0$ base,

$$\mu(X_{1^{+-}}(6137)) = \left(\sqrt{\tfrac{1}{6}} \quad \sqrt{\tfrac{1}{6}} \right)$$

in the $|[c\bar{c}]^1_1\{c\bar{c}\}^1_0\rangle^1_1$, $|\{c\bar{c}\}^1_0[c\bar{c}]^1_1\rangle^1_1$ base, and

$$\mu(X_{2^{++}}(6194)) = \sqrt{\tfrac{1}{3}}$$

in the $|\{c\bar{c}\}^1_1\{c\bar{c}\}^1_1\rangle^1_2$ base. By expanding explicitly, one obtains

$$X_{0^{++}}(6035) \sim \left(\sqrt{\tfrac{1}{6}}\beta_{11} + \tfrac{1}{2}\beta_{12} \right) |[c\bar{c}]^1_0[c\bar{c}]^1_0\rangle^1_0$$
$$+ \left(\sqrt{\tfrac{1}{2}}\beta_{11} - \tfrac{1}{2\sqrt{3}}\beta_{12} \right) |\{c\bar{c}\}^1_1\{c\bar{c}\}^1_1\rangle^1_0, \tag{20}$$

$$X_{0^{++}}(6254) \sim \left(\sqrt{\tfrac{1}{6}}\beta_{21} + \tfrac{1}{2}\beta_{22} \right) |[c\bar{c}]^1_0[c\bar{c}]^1_0\rangle^1_0$$
$$+ \left(\sqrt{\tfrac{1}{2}}\beta_{21} - \tfrac{1}{2\sqrt{3}}\beta_{22} \right) |\{c\bar{c}\}^1_1\{c\bar{c}\}^1_1\rangle^1_0, \tag{21}$$

$$X_{1^{+-}}(6137) \sim \sqrt{\tfrac{1}{6}}|[c\bar{c}]^1_1\{c\bar{c}\}^1_0\rangle^1_1 + \sqrt{\tfrac{1}{6}}|\{c\bar{c}\}^1_0[c\bar{c}]^1_1\rangle^1_1, \tag{22}$$

$$X_{2^{++}}(6194) \sim \sqrt{\tfrac{1}{3}}|\{c\bar{c}\}^1_1\{c\bar{c}\}^1_1\rangle^1_2, \tag{23}$$

with their masses in $(\cdots)$. Here the values in $(\cdots)$ are the bare pole masses before the coupled channel effect which will be discussed in the next section. With the definitions

$$g_{\text{di-}J/\psi} := \langle J/\psi J/\psi | \hat{H}_{\text{strong}} | | \{c\bar{c}\}^1_1\{c\bar{c}\}^1_1\rangle^1_J\rangle, \tag{24}$$

$$g_{\text{di-}\eta_c} := \langle \eta_c\eta_c | \hat{H}_{\text{strong}} | | [c\bar{c}]^1_0[c\bar{c}]^1_0\rangle^1_J\rangle \tag{25}$$

TABLE IV. The Hamiltonian (the third column) in the bases listed in Table I, and predicted mass spectra (the forth and fifth columns) for the $cc\bar{c}\bar{c}$, $bb\bar{b}\bar{b}$, and $bc\bar{b}\bar{c}$ tetraquarks with various J^{PC}'s as well as their corresponding eigenvectors (the last column).

J^{PC}	Tetraquark	H [MeV]	Mass [MeV]	Error [MeV]	Eigenvector
0^{++}	$cc\bar{c}\bar{c}$	$\begin{bmatrix} 6179.68 & -103.80 \\ -103.80 & 6109.05 \end{bmatrix}$	$\begin{bmatrix} 6034.72 \\ 6254.00 \end{bmatrix}$	$\begin{bmatrix} 0.52 \\ 0.57 \end{bmatrix}$	$\begin{bmatrix} 0.58 & 0.81 \\ -0.81 & 0.58 \end{bmatrix}$
	$bb\bar{b}\bar{b}$	$\begin{bmatrix} 18912.91 & -56.58 \\ -56.58 & 18874.41 \end{bmatrix}$	$\begin{bmatrix} 18833.90 \\ 18953.43 \end{bmatrix}$	$\begin{bmatrix} 2.12 \\ 2.34 \end{bmatrix}$	$\begin{bmatrix} 0.58 & 0.81 \\ -0.81 & 0.58 \end{bmatrix}$
	$bc\bar{b}\bar{c}$	$\begin{bmatrix} 12463.09 & 0 & 0 & -65.36 \\ 0 & 12579.53 & -65.36 & 0 \\ 0 & -65.36 & 12582.44 & 0 \\ -65.36 & 0 & 0 & 12563.01 \end{bmatrix}$	$\begin{bmatrix} 12515.61 \\ 12646.36 \\ 12430.79 \\ 12595.32 \end{bmatrix}$	$\begin{bmatrix} 6.75 \\ 8.94 \\ 12.14 \\ 8.41 \end{bmatrix}$	$\begin{bmatrix} 0 & 0.71 & 0.70 & 0 \\ 0 & -0.70 & 0.71 & 0 \\ 0.90 & 0 & 0 & 0.44 \\ -0.44 & 0 & 0 & 0.90 \end{bmatrix}$
1^{+-}	$cc\bar{c}\bar{c}$	$[6137.30]$	$[6137.30]$	$[0.25]$	$[1]$
	$bb\bar{b}\bar{b}$	$[18889.81]$	$[18889.81]$	$[1.07]$	$[1]$
	$bc\bar{b}\bar{c}$	$\begin{bmatrix} 12338.56 & 0 & 0 & 0 \\ 0 & 12369.28 & 0 & -37.73 \\ 0 & 0 & 12572.73 & 0 \\ 0 & -37.73 & 0 & 12590.51 \end{bmatrix}$	$\begin{bmatrix} 12363.02 \\ 12596.77 \\ 12338.56 \\ 12572.72 \end{bmatrix}$	$\begin{bmatrix} 9.88 \\ 8.49 \\ 9.87 \\ 9.10 \end{bmatrix}$	$\begin{bmatrix} 0 & 0.99 & 0 & 0.16 \\ 0 & -0.16 & 0 & 0.99 \\ 1 & 0 & 0 & 0 \\ 0 & 0 & 1 & 0 \end{bmatrix}$
1^{++}	$bc\bar{b}\bar{c}$	$\begin{bmatrix} 12565.78 & 37.73 \\ 37.73 & 12590.51 \end{bmatrix}$	$\begin{bmatrix} 12538.44 \\ 12617.85 \end{bmatrix}$	$\begin{bmatrix} 6.14 \\ 7.00 \end{bmatrix}$	$\begin{bmatrix} -0.81 & 0.59 \\ 0.59 & 0.81 \end{bmatrix}$
2^{++}	$cc\bar{c}\bar{c}$	$[6193.80]$	$[6193.80]$	$[0.35]$	$[1]$
	$bb\bar{b}\bar{b}$	$[18920.61]$	$[18920.61]$	$[1.47]$	$[1]$
	$bc\bar{b}\bar{c}$	$\begin{bmatrix} 12596.50 & 0 \\ 0 & 12612.83 \end{bmatrix}$	$\begin{bmatrix} 12596.50 \\ 12612.83 \end{bmatrix}$	$\begin{bmatrix} 4.57 \\ 8.71 \end{bmatrix}$	$\begin{bmatrix} 1 & 0 \\ 0 & 1 \end{bmatrix}$

indicating the hadronization process, one can obtain the relative transition rate to di-J/ψ is

$$|\mathcal{M}(X_{2^{++}}^{\text{di-}J/\psi}(6194))|^2 : |\mathcal{M}(X_{0^{++}}^{\text{di-}J/\psi}(6254))|^2 : |\mathcal{M}(X_{0^{++}}^{\text{di-}J/\psi}(6035))|^2$$

$$= \frac{1}{3}g_{\text{di-}J/\psi}^2 : \left(\sqrt{\frac{1}{2}}\beta_{21} - \frac{1}{2\sqrt{3}}\beta_{22}\right)^2 g_{\text{di-}J/\psi}^2 : \left(\sqrt{\frac{1}{2}}\beta_{11} - \frac{1}{2\sqrt{3}}\beta_{12}\right)^2 g_{\text{di-}J/\psi}^2 \sim 33:55:3 \qquad (26)$$

and that to di-η_c is

$$|\mathcal{M}(X_{0^{++}}^{\text{di-}\eta_c}(6254))|^2 : |\mathcal{M}(X_{0^{++}}^{\text{di-}\eta_c}(6035))|^2$$

$$= \left(\sqrt{\frac{1}{6}}\beta_{21} + \frac{1}{2}\beta_{22}\right)^2 g_{\text{di-}\eta_c}^2 : \left(\sqrt{\frac{1}{6}}\beta_{11} + \frac{1}{2}\beta_{12}\right)^2 g_{\text{di-}\eta_c}^2$$

$$\sim 0:41. \qquad (27)$$

Although the hadronization parameters do not play a role here, they will when the coupled channel effect is included. Considering the S-wave phase space

$$\text{P.S.} = \frac{1}{8\pi}\frac{|\boldsymbol{p}|}{M^2} \qquad (28)$$

with $|\boldsymbol{p}|$ the three momentum of the final particle in the rest frame of the decaying tetraquark, the ratio to di-η_c becomes $1:127$. It means that the lower $X_{0^{++}}(6035)$ should be more significant in the di-η_c channel, which is also the case after the coupled channel effect. After inclusion of the S-wave phase space, only the $X_{0^{++}}(6254)$ is allowed to decay into

di-J/ψ and would be expected to be significant in the di-J/ψ lineshape.

C. Coupled channel effect to two hidden charmonium channels

From Eqs. (20)–(25) one also can obtain the potentials between two hidden charmonium channels via bare tetraquark poles in the above subsection. As the allowed C-parity of the di-J/ψ system is positive, only the 0^{++} and 2^{++} quantum numbers could explain the structure in experiment [12]. For the 0^{++} channel, we consider the $\eta_c\eta_c$, $J/\psi J/\psi$, $J/\psi\psi'$, and $J/\psi\psi(3770)$ channels. The inclusion of the latter two is because of the significant changes in the lineshape. The corresponding 0^{++} potential reads as

$$V_{ij}^{0^{++}}(E) = \sum_{n=1,2}\sum_{\alpha,\beta=1,2} \frac{\mu_n^\alpha \mu_n^\beta g_i^\alpha g_j^\beta}{E - E_{n0}} \qquad (29)$$

with E_{10} and E_{20}, the masses of bare compact fully heavy tetraquarks $X_{0^{++}}(6035)$ and $X_{0^{++}}(6254)$, respectively. μ_n^α
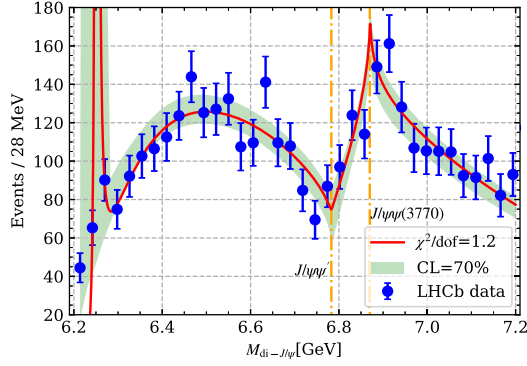
FIG. 3. The fitted result (red solid curve) compared to the experimental data [12]. The band is the error with 70% confidence level. The two orange vertical lines are the $J/\psi\psi'$ and the $J/\psi\psi(3770)$ thresholds.

is the coefficient of the $|[c\bar{c}]^1_0[c\bar{c}]^1_0\rangle^1_0$, $|\{c\bar{c}\}^1_1\{c\bar{c}\}^1_1\rangle^1_0$ components of the nth compact tetraquarks. g^α_i represents the αth component hadronization to the ith channel [analogous to Eqs. (24) and (25)]. For the 2^{++} channel, we have $J/\psi J/\psi$, $J/\psi\psi'$, and $J/\psi\psi(3770)$ channels and the corresponding potential can be obtained analogous to Eq. (29).

The two-body propagator for the ith channel is

$$G_i(E) = \frac{1}{16\pi^2}\left\{ a(\mu) + \log\frac{m^2_{i1}}{\mu^2} + \frac{m^2_{i2} - m^2_{i1} + s}{2s}\log\frac{m^2_{i2}}{m^2_{i1}} \right.$$
$$+ \frac{k}{E}[\log(2k_iE + s + \Delta_i) + \log(2k_iE + s - \Delta_i)$$
$$\left. - \log(2k_iE - s + \Delta_i) - \log(2k_iE - s - \Delta_i)]\right\} \quad (30)$$

where $s = E^2$, m_{i1} and m_{i2} are the particle masses in the ith channel, and $\Delta_i = m^2_{i1} - m^2_{i2}$, $k_i = \lambda^{1/2}(E^2, m^2_{i1}, m^2_{i2})/2E$. Here the dimensional regularization is used to regularize the ultradivergence and we take $a(\mu) = -3$, $\mu = 1$ GeV. The physical scattering T matrix can be obtained by solving Lippmann-Schwinger equation

$$T = V + VGT. \quad (31)$$

The physical production amplitude of double J/ψ is

$$P^{0^{++}}_2 = U^{0^{++}}_2 + U^{0^{++}}_1 G_1T_{12} + U^{0^{++}}_2 G_2T_{22} + U^{0^{++}}_3 G_3T_{32}$$
$$+ U^{0^{++}}_4 G_4T_{42} \quad (32)$$

where $U^{0^{++}}_i$ stands for the bare production amplitude for the ith channel with $J^{PC} = 0^{++}$. Notice that the channels $\eta_c\eta_c$, $J/\psi J/\psi$, $J/\psi\psi'$, and $J/\psi\psi(3770)$ are ordered by their thresholds. Analogously, the physical production amplitude of di-J/ψ for the 2^{++} state is

TABLE V. The values of the parameters extracted from the fit. The errors are from the experimental uncertainties. The subscripts are for the corresponding channels.

Parameters	0^{++}	2^{++}
$U^{J^{PC}}_{\eta_c\eta_c}$	-572.92 ± 912.33	$\cdots$
$U^{J^{PC}}_{J/\psi J/\psi}$	7.53 ± 3.87	30.67 ± 1.93
$U^{J^{PC}}_{J/\psi\psi'}$	34447.71 ± 4145.37	39111.96 ± 6605.72
$U^{J^{PC}}_{J/\psi\psi''}$	-37513.64 ± 4035.80	-51446.38 ± 7192.27
$g_{J/\psi J/\psi}$	0.989 ± 0.03	
$g_{\eta_c\eta_c}$	0.924 ± 0.03	
$g_{J/\psi\psi'}$	0.177 ± 0.02	
$g_{J/\psi\psi''}$	0.134 ± 0.01	

$$P^{2^{++}}_1 = U^{2^{++}}_1 + U^{2^{++}}_1 G_1T_{11} + U^{2^{++}}_2 G_2T_{21} + U^{2^{++}}_3 G_3T_{31}.$$

Here, G_i represents the two-loop function of $J/\psi J/\psi$, $J/\psi\psi'$, and $J/\psi\psi(3770)$ and $U^{2^{++}}_i$ stands for the bare production amplitude for the ith channel with $J^{PC} = 2^{++}$. We adopt the S-wave phase space factor

$$\rho(E) = \frac{|\boldsymbol{k}|}{8\pi E}, \quad (33)$$

with $|\boldsymbol{k}|$ the three momentum of the particle in the center-of-rest frame, similar to Ref. [48]. The final fit function is

$$(|P^{0^{++}}_2|^2 + |P^{2^{++}}_1|^2)\rho(E). \quad (34)$$

The fitted di-J/ψ invariant mass distribution comparing to the experimental data is shown in Fig. 3, with the fitted parameters in Table V. From the figure, one can see a significant structure around 6.25 GeV which might stem from the shifted $X_{0^{++}}(6254)$. This structure could be seen when the experimental statistic increases and can be viewed as strong evidence of the compact fully heavy tetraquarks. The structure around 6.9 GeV demonstrates itself as a cusp effect from the $J/\psi\psi(3770)$ channel. As stated in the above section, the bare $X_{0^{++}}(6035)$ strongly couples to the di-η_c channel and will demonstrate itself in this channel. In addition, even after the coupled channel effect, the shift of this bare state is marginal. That means the results for the bare pole almost survive and the $X_{0^{++}}(6035)$ will also show a significant peak structure in the di-η_c spectrum, which is a key physical observable for the nature of the fully heavy tetraquark. For the further measurement in experiment, the di-η_c lineshape is presented in Fig. 4 without any background.

To further check this understanding, the pole positions of the corresponding S-matrix are extracted and shown in Table VI, comparing them to the bare pole masses.[1]

---

[1]The pole positions have also been extracted in Refs. [48–50] based on the molecular picture, which might have different quantum numbers compared with the compact ones here. As the result, the comparison with their results are not presented.
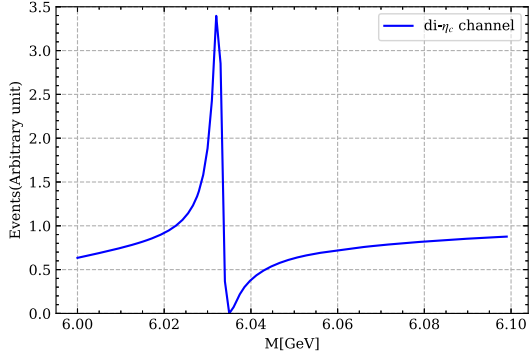
FIG. 4. Prediction of the di-η_c lineshape.
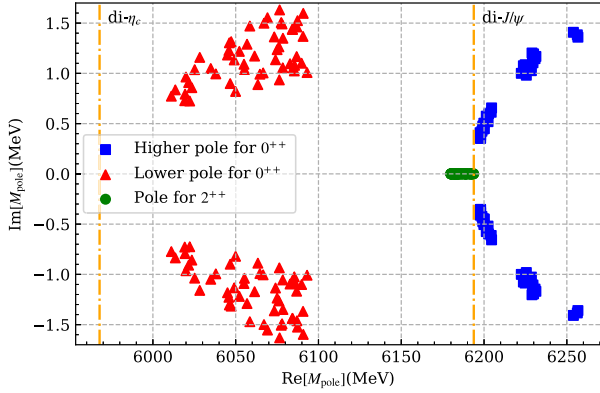
FIG. 5. Pole positions of the 0^{++} (red triangles and blue boxes for the lower and higher ones, respectively) and 2^{++} (green circles) channels with parameters with 70% confidence level. The yellow dashed vertical lines are the di-η_c and di-J/ψ channels, respectively.

One can see that the shift of the pole positions to the bare masses are tiny, which indicates that the physical states are dominated by compact tetraquarks. We do not find a pole around 6.9 GeV which indicates that the structure is only the cusp effect from the $J/\psi\psi(3770)$ channel. One can also see a dip structure in Fig. 3 around the $J/\psi\psi'$ threshold. The pole positions with the parameters within 70% confidence level are shown in Fig. 5. The two 0^{++} tetraquarks behave as two resonances above the di-η_c and di-J/ψ thresholds, respectively. The 2^{++} state is a bound state below the di-J/ψ threshold. The positions of these three states are listed in Table VI comparing them with the bare pole masses. In addition, the nature of full-charm tetraquark

TABLE VII. The scattering length a_0, effective range r_0 in the di-J/ψ channel, as well as the corresponding compositeness $\bar{X}_A$ and wave function renormalization constants $\bar{Z}_A$ for the 0^{++} and 2^{++} channels. The errors are from the uncertainties of the experimental data.

	0^{++}	2^{++}
a_0 (fm)	$0.012^{+3.129}_{-5.142}$	$-0.280^{+0.443}_{-2.397}$
r_0 (fm)	$-37.966^{+4.010}_{-4.882}$	$-60.803^{+1.592}_{-15.222}$
$\bar{X}_A$	$0.013^{+0.241}_{-0.003}$	$0.048^{+0.095}_{-0.042}$
$\bar{Z}_A$	$0.987^{+0.003}_{-0.241}$	$0.952^{+0.042}_{-0.095}$

states can also be obtained by estimating their composite-ness $\bar{X}_A = 1 - \overline{Z}_A$ [48,56] with $\overline{Z}_A = 1$ for molecules and $\bar{Z}_A = 0$ for compact states, respectively. This idea was proposed by Weinberge in 1963 for bound states [73] and extended to virtual states and resonances [56,74] recently. Practically, the di-J/ψ to di-J/ψ scattering amplitude can be parametrized in the effective range expansion

$$T(k) = -8\pi\sqrt{s}\left[\frac{1}{a_0} + \frac{1}{2}r_0k^2 - ik + \mathcal{O}(k^4)\right]^{-1}, \quad (35)$$

with a_0, r_0 the scattering length and effective range, respectively. k is the three momentum of the J/ψ in the di-J/ψ center-of-mass frame. By comparing with the physical scattering amplitude, one can extract the S-wave scattering length a_0 and the effective range r_0. Furthermore, one can obtain the compositeness [56]

$$\bar{X}_A = \frac{1}{\sqrt{1 + 2|r_0/a_0|}}. \quad (36)$$

The results are collected in Table VII. The absolute values of the effective range are much larger than those of the scattering lengths for both 0^{++} and 2^{++} channels. That indicates that compact tetraquarks are the dominant con-tributions which can also be understood by the large values of $\bar{Z}_A$ in Table VII. This behavior has also been explained by the frame with the so-called Castillejo-Dalitz-Dyson (CDD) pole [50,75,76], which states that the scattering length a_0 and effective range r_0 should be linearly and quadratically inversely proportional to the distance between the CDD pole M_{CDD} and the relevant threshold $m_{thr.}$, respectively, i.e.,

TABLE VI. The pole positions of the 0^{++} and 2^{++} channels compared with the bare tetraquark masses in the bracket. The errors of the pole positions inherit from the experimental errors of the di-J/ψ invariant mass distribution.

	0^{++}	2^{++}
Poles (MeV)	$6251.65^{+5}_{-54} + 1.47^{+0.06}_{-1.12}i \ (6254^{+0.57}_{-0.57})$	$6192.46^{+1.23}_{-12.56} \ (6193.8^{+0.35}_{-0.35})$
	$6032.96^{+60.16}_{-21.82} + 1.036^{+0.60}_{-0.31}i \ (6034.72^{+0.52}_{-0.52})$	

$$a_0 \propto M_{\text{CDD}} - m_{\text{thr}}, \qquad r_0 \propto (M_{\text{CDD}} - m_{\text{thr}})^{-2}. \quad (37)$$

To get a whole picture of the fully heavy tetraquark system, we compare our results with those presented in Refs. [16,26–29,46,66,69,77] in the compact tetraquark picture. Figure 6 is the comparison of the spectra from these works. For the full-charm tetraquark system $cc\bar{c}\bar{c}$, the spectra has been obtained with the parametrization scheme in Refs. [27,28,66] and our work, Gaussian expansion method [78] in Refs. [16,26,29,46], and QCD sum rules in Refs. [69,77]. The masses of the full-charm tetraquarks mostly fall in the internal [6.2, 6.8] GeV, which are in a good agreement with the range of mass for the broad

structure investigated by LHCb [12]. In Ref. [28], the mass splitting is dominated only by the spin interaction. References [6,20,66] further include the chromoelectric and chromomagnetic interactions and find that these two kinds of interactions cannot be neglected to obtain the correct spectrum. Among them, our method is similar to that in Ref. [27] and our results should be consistent with each other. However, one can see a deviation from Fig. 6, which could stem from the different methods of extracting the parameters. Our framework is under non-relativistic approximation and the kinematic terms have been ignored compared with the heavy quark mass terms and chromoelectric/chromomagnetic interaction.
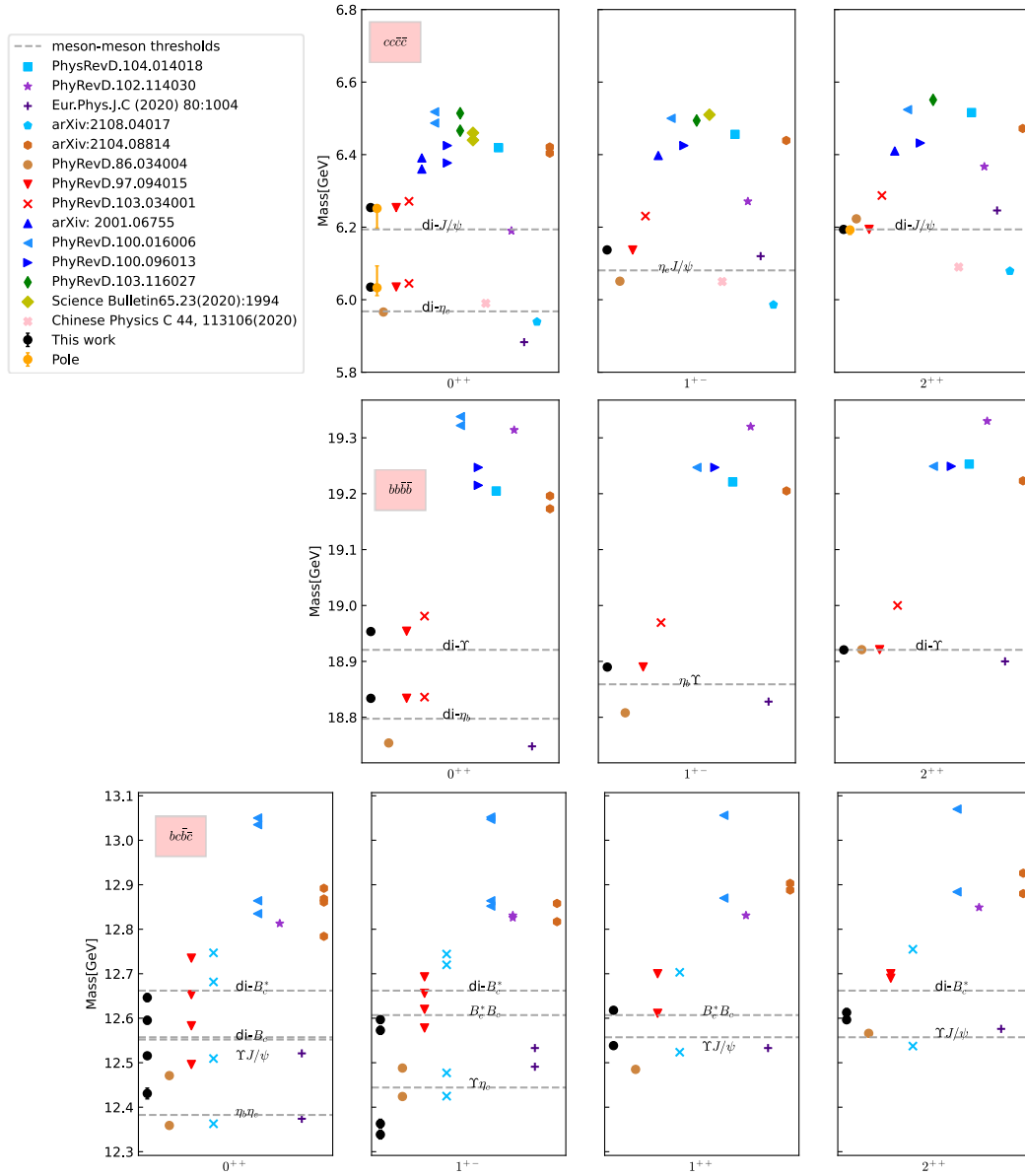

FIG. 6. Comparison of the fully heavy tetraquark spectra (in units of GeV) with other works [16,26–29,32,35,36,38,41,46,66,69,77]. The black circles are for the compact fully heavy tetraquarks. The yellow circles in the $cc\bar{c}\bar{c}$ spectra are the pole positions. The gray dashed lines are for the thresholds of potential two-charmonium decay channels.

For Refs. [27,79] both the light meson and heavy meson masses are used to extract the parameters, which is the reason for the deviation. The spectra can also be obtained by solving the Schrödinger equation numerically with the variational method [16,26,29,46], which can only give the upper limits of the system. It is the reason why the masses with the variational method is much larger than those with the parametrization ones [27,79] and ours. The QCD sum rule can also be used to obtain the spectra [69,77] of the fully heavy system. Reference [69] concludes that the broad structure around 6.2–6.8 GeV and $X(6900)$ is an S-wave and a P-wave full-charm tetraquark states, respectively. On the contrary, Ref. [77] shows that the broad structure is the first radial excited state of the $cc\bar{c}\bar{c}$ tetraquark and the $X(6900)$ is the second radial excited state of $cc\bar{c}\bar{c}$ tetraquark.

IV. SUMMARY

In this work, we first extract the internal structure of the fully heavy tetraquarks directly from the experimental data, within the compact tetraquark picture. The bare pole masses are obtained from the parametrization with both chromoelectric and chromomagnetic interactions. For the S-wave ground states, the spacial wave function is trivial and their overlapping can be neglected. The rest parameters are extracted from the masses of the S-wave ground heavy mesons, i.e., the J/ψ, η_c, $\Upsilon(1S)$, $\eta_b(1S)$, B_c and B_c^*. Most of the bare masses are above the lowest allowed two-heavy-quarkonium decay channels. However, it does not mean that all of them could exhibit themselves as broader structures in the lineshape. For an illustration, although the $X_{0^{++}}(6035)$ mass is smaller than the $X_{0^{++}}(6254)$, its transition to the di-η_c channel is much larger than that of the

$X_{0^{++}}(6254)$. This makes the $X_{0^{++}}(6035)$ more significant in the di-η_c lineshape even after the coupled channel effect. This is an unique feature which can distinguish compact $cc\bar{c}\bar{c}$ tetraquark from the loosely hadronic molecule. After a fit to the di-J/ψ lineshape, we find that the $X(6900)$ reported by LHCb is only a cusp effect from the $J/\psi\psi(3770)$ channel. In addition, there is also a cusp effect slightly below 6.8 GeV stemming from the $J/\psi\psi'$ channel. The two 0^{++} tetraquarks behave as two resonances above the di-η_c and di-J/ψ thresholds, respectively. The 2^{++} state is a bound state below the di-J/ψ threshold. Studying the lineshape from the compact tetraquark picture and comparing them with those from the molecular picture can tell how much we have learnt from the experimental data and where we should go.

[1] H. X. Chen, W. Chen, X. Liu, and S. L. Zhu, Phys. Rep. **639,** 1 (2016).

[2] H. X. Chen, W. Chen, X. Liu, Y. R. Liu, and S. L. Zhu, Rep. Prog. Phys. **80,** 076201 (2017).

[3] Y. Dong, A. Faessler, and V. E. Lyubovitskij, Prog. Part. Nucl. Phys. **94,** 282 (2017).

[4] R. F. Lebed, R. E. Mitchell, and E. S. Swanson, Prog. Part. Nucl. Phys. **93,** 143 (2017).

[5] F. K. Guo, C. Hanhart, U.-G. Meißner, Q. Wang, Q. Zhao, and B. S. Zou, Rev. Mod. Phys. **90,** 015004 (2018).

[6] Y. R. Liu, H. X. Chen, W. Chen, X. Liu, and S. L. Zhu, Prog. Part. Nucl. Phys. **107,** 237 (2019).

[7] R. M. Albuquerque, J. M. Dias, K. P. Khemchandani, A. Martínez Torres, F. S. Navarra, M. Nielsen, and C. M. Zanetti, J. Phys. G **46,** 093002 (2019).

[8] Y. Yamaguchi, A. Hosaka, S. Takeuchi, and M. Takizawa, J. Phys. G **47,** 053001 (2020).

[9] F. K. Guo, X. H. Liu, and S. Sakai, Prog. Part. Nucl. Phys. **112,** 103757 (2020).

[10] N. Brambilla, S. Eidelman, C. Hanhart, A. Nefediev, C. P. Shen, C. E. Thomas, A. Vairo, and C. Z. Yuan, Phys. Rep. **873,** 1 (2020).

[11] R. Aaij *et al.* (LHCb Collaboration), J. High Energy Phys. 10 (2018) 086.

[12] R. Aaij *et al.* (LHCb Collaboration), Sci. Bull. **65,** 1983 (2020).

[13] A. M. Sirunyan *et al.* (CMS Collaboration), Phys. Lett. B **808,** 135578 (2020).

[14] Y. Iwasaki, Prog. Theor. Phys. **54,** 492 (1975).

[15] K. T. Chao, Z. Phys. C **7,** 317 (1981).

[16] Z. Zhao, K. Xu, A. Kaewsnod, X. Liu, A. Limphirat, and Y. Yan, Phys. Rev. D **103,** 116027 (2021).

[17] R. N. Faustov, V. O. Galkin, and E. M. Savchenko, Universe **7,** 94 (2021).

[18] Q. F. Lü, D. Y. Chen, and Y. B. Dong, Eur. Phys. J. C **80,** 871 (2020).
[19] M. Karliner, S. Nussinov, and J. L. Rosner, Phys. Rev. D **95,** 034011 (2017).
[20] C. Deng, H. Chen, and J. Ping, Phys. Rev. D **103,** 014001 (2021).
[21] W. Chen, H. X. Chen, X. Liu, T. G. Steele, and S. L. Zhu, Phys. Lett. B **773,** 247 (2017).
[22] J. Zhao, S. Shi, and P. Zhuang, Phys. Rev. D **102,** 114001 (2020).
[23] H. W. Ke, X. Han, X. H. Liu, and Y. L. Shi, Eur. Phys. J. C **81,** 427 (2021).
[24] R. Zhu, Nucl. Phys. **B966,** 115393 (2021).
[25] M. Karliner and J. L. Rosner, Phys. Rev. D **102,** 114039 (2020).
[26] G. J. Wang, L. Meng, and S. L. Zhu, Phys. Rev. D **100,** 096013 (2019).
[27] X. Z. Weng, X. L. Chen, W. Z. Deng, and S. L. Zhu, Phys. Rev. D **103,** 034001 (2021).
[28] A. V. Berezhnoy, A. V. Luchinsky, and A. A. Novoselov, Phys. Rev. D **86,** 034004 (2012).
[29] X. Chen, arXiv:2001.06755.
[30] R. Maciuła, W. Schäfer, and A. Szczurek, Phys. Lett. B **812,** 136010 (2021).
[31] B. D. Wan and C. F. Qiao, Phys. Lett. B **817,** 136339 (2021).
[32] G. Yang, J. Ping, and J. Segovia, Phys. Rev. D **104,** 014006 (2021).
[33] J. M. Richard, Nucl. Part. Phys. Proc. **312–317,** 146 (2021).
[34] A. Szczurek, R. Maciuła, and W. Schäfer, arXiv:2107.13285.
[35] R. Tiwari, D. P. Rathaud, and A. K. Rai, arXiv:2108.04017.
[36] M. A. Bedolla, J. Ferretti, C. D. Roberts, and E. Santopinto, Eur. Phys. J. C **80,** 1004 (2020).
[37] A. V. Nefediev, Eur. Phys. J. C **81,** 692 (2021).
[38] R. N. Faustov, V. O. Galkin, and E. M. Savchenko, Phys. Rev. D **102,** 114030 (2020).
[39] X. Y. Wang, Q. Y. Lin, H. Xu, Y. P. Xie, Y. Huang, and X. Chen, Phys. Rev. D **102,** 116014 (2020).
[40] G. Huang, J. Zhao, and P. Zhuang, Phys. Rev. D **103,** 054014 (2021).
[41] Q. Li, C. H. Chang, G. L. Wang, and T. Wang, Phys. Rev. D **104,** 014018 (2021).
[42] G. J. Wang, L. Meng, M. Oka, and S. L. Zhu, Phys. Rev. D **104,** 036016 (2021).
[43] J. Sonnenschein and D. Weissman, Eur. Phys. J. C **81,** 25 (2021).
[44] G. Yang, J. Ping, and J. Segovia, Symmetry **12,** 1869 (2020).
[45] F. X. Liu, M. S. Liu, X. H. Zhong, and Q. Zhao, Phys. Rev. D **104,** 116029 (2021).
[46] M. S. Liu, Q. F. Lü, X. H. Zhong, and Q. Zhao, Phys. Rev. D **100,** 016006 (2019).
[47] M. S. liu, F. X. Liu, X. H. Zhong, and Q. Zhao, arXiv:2006.11952.
[48] X. K. Dong, V. Baru, F. K. Guo, C. Hanhart, and A. Nefediev, Phys. Rev. Lett. **126,** 132001 (2021); **127,** 119901(E) (2021).

[49] Z. R. Liang, X. Y. Wu, and D. L. Yao, Phys. Rev. D **104,** 034034 (2021).
[50] Z. H. Guo and J. A. Oller, Phys. Rev. D **103,** 034024 (2021).
[51] X. K. Dong, V. Baru, F. K. Guo, C. Hanhart, A. Nefediev, and B. S. Zou, Sci. Bull. **66,** 2462 (2021).
[52] J. Z. Wang, X. Liu, and T. Matsuki, Phys. Lett. B **816,** 136209 (2021).
[53] Q. F. Cao, H. Chen, H. R. Qi, and H. Q. Zheng, Chin. Phys. C **45,** 103102 (2021).
[54] J. Z. Wang, D. Y. Chen, X. Liu, and T. Matsuki, Phys. Rev. D **103,** L071503 (2021).
[55] C. Gong, M. C. Du, Q. Zhao, X. H. Zhong, and B. Zhou, Phys. Lett. B **824,** 136794 (2022).
[56] I. Matuschek, V. Baru, F. K. Guo, and C. Hanhart, Eur. Phys. J. A **57,** 101 (2021).
[57] F. Abe *et al.* (CDF Collaboration), Phys. Rev. D **58,** 112004 (1998).
[58] M. McNeil (ALEPH Collaboration), Int. J. Mod. Phys. A **12,** 3921 (1997).
[59] P. G. Ortega, J. Segovia, D. R. Entem, and F. Fernandez, Eur. Phys. J. C **80,** 223 (2020).
[60] D. Griffiths, *Introduction to Elementary Particles* (Wiley, 2008).
[61] S. Meinel, Phys. Rev. D **82,** 114514 (2010).
[62] M. Padmanath, R. G. Edwards, N. Mathur, and M. Peardon, Phys. Rev. D **90,** 074504 (2014).
[63] N. Mathur, M. Padmanath, and S. Mondal, Phys. Rev. Lett. **121,** 202002 (2018).
[64] P. A. Zyla *et al.* (Particle Data Group), Prog. Theor. Exp. Phys. **2020,** 083C01 (2020).
[65] J. P. Ader, J. M. Richard, and P. Taxil, Phys. Rev. D **25,** 2370 (1982).
[66] J. Wu, Y. R. Liu, K. Chen, X. Liu, and S. L. Zhu, Phys. Rev. D **97,** 094015 (2018).
[67] J. R. Zhang, Phys. Rev. D **103,** 014018 (2021).
[68] B. C. Yang, L. Tang, and C. F. Qiao, Eur. Phys. J. C **81,** 324 (2021).
[69] H. X. Chen, W. Chen, X. Liu, and S. L. Zhu, Sci. Bull. **65,** 1994 (2020).
[70] C. Becchi, A. Giachino, L. Maiani, and E. Santopinto, Phys. Lett. B **806,** 135495 (2020).
[71] C. Becchi, J. Ferretti, A. Giachino, L. Maiani, and E. Santopinto, Phys. Lett. B **811,** 135952 (2020).
[72] A. Ali, L. Maiani, and A. D. Polosa, *Multiquark Hadrons* (Cambridge University Press, Cambridge, England, 2019).
[73] S. Weinberg, Phys. Rev. **130,** 776 (1963).
[74] V. Baru, J. Haidenbauer, C. Hanhart, Y. Kalashnikova, and A. E. Kudryavtsev, Phys. Lett. B **586,** 53 (2004).
[75] Z. H. Guo and J. A. Oller, Phys. Rev. D **93,** 054014 (2016).
[76] X. W. Kang, Z. H. Guo, and J. A. Oller, Phys. Rev. D **94,** 014012 (2016).
[77] Z. G. Wang, Chin. Phys. C **44,** 113106 (2020).
[78] E. Hiyama, Prog. Theor. Exp. Phys. **2012,** 01A204 (2012).
[79] X. Z. Weng, X. L. Chen, and W. Z. Deng, Phys. Rev. D **97,** 054008 (2018).